Synergistic Adsorption of Cd(II) with Sulfate/Phosphate on Ferrihydrite: An *in Situ* ATR-FTIR/2D-COS Study

Jing Liu[1,2,3], Runliang Zhu[1,2]*, Xiaoliang Liang[1,2], Lingya Ma[1,2], Xiaoju Lin[1,2,3], Jianxi Zhu[1,2], Hongping He[1,2,3], Stephen C. Parker[4], Marco Molinari[5,4]

1. *Key Laboratory of Mineralogy and Metallogeny, Guangzhou Institute of Geochemistry, Chinese Academy of Sciences, Guangzhou 510640, China*
2. *Guangdong Provincial Key Laboratory of Mineral Physics and Material Research & Development, Guangzhou 510640, China*
3. *University of Chinese Academy of Sciences, Beijing 100049, China*
4. *Department of Chemistry, University of Bath, Claverton Down, Bath, BA2 7AY, UK*
5. *Department of Chemistry, University of Huddersfield, Queensgate, Huddersfield HD1 3DH, UK*

* Corresponding author

Phone: 86-020-85297603

Fax: 86-020-85297603

E-mail: zhurl@gig.ac.cn

Abstract

Elucidation of the co-adsorption characteristics of heavy metal cations and oxyanions on (oxyhydr)oxides can help to better understand their distribution and transformation in many geological settings. In this work, batch adsorption experiments in combination with *in situ* attenuated total reflectance Fourier transform infrared spectroscopy (ATR-FTIR) were applied to explore the interaction mechanisms of Cd(II) with sulfate or phosphate at the ferrihydrite (Fh)−water interface, and the two-dimensional correlation spectroscopic analysis (2D-COS) was used to enhance the resolution of ATR-FTIR bands and the accuracy of analysis. The batch adsorption experiments showed enhanced adsorption of both sulfate (S) and phosphate (P) on Fh when co-adsorbed with Cd(II); additionally, the desorbed percentages of Cd(II) were much lower in the P+Cd adsorption systems than those in the S+Cd adsorption systems. The spectroscopic results suggested that in the single adsorption systems, sulfate primarily adsorbed as outer-sphere complexes with a small amount of bidentate inner-sphere complexes, while the dominant adsorbed species of phosphate were largely the bidentate nonprotonated inner-sphere complexes, although there was significant pH-dependence. In the co-adsorption systems, the synergistic adsorption of Cd(II) and sulfate was dominantly attributed to the electrostatic interaction, as well as the formation of Fe−Cd−S (i.e., Cd-bridged) ternary complexes. In contrast, Fe−P−Cd (i.e., phosphate-bridged) ternary complexes were found in all of the co-adsorption systems of phosphate and Cd(II); furthermore, electrostatic interaction should also contribute to the co-adsorption process. Our results show that *in situ* ATR-FTIR in combination with 2D-COS can be an efficient tool in analyzing the co-adsorption mechanisms of anions and heavy metal cations on iron (oxyhydr)oxides in ternary adsorption systems. The co-existence of Cd(II) with sulfate or phosphate can be beneficial for their accumulations on Fh, and phosphate is more efficient than sulfate for the long-term immobilization of Cd(II).

Keywords: Cadmium; Phosphate; Sulfate; Ferrihydrite; Synergistic adsorption; ATR-FTIR; 2D-COS

1. Introduction

Iron (oxyhydr)oxides can significantly affect the speciation and distribution of contaminants, nutrients, and other solutes in water−rock systems through adsorption processes and thus control the geochemical cycle of many elements.[1-6] The complexity of natural geomedia implies that the adsorption of multiple components may occur simultaneously. In recent years, the co-adsorption of heavy metal cations and oxyanions has attracted interest in geochemistry and environmental science.[7-11] Although a few studies have shown that the adsorption of heavy metal cations and oxyanions on iron (oxyhydr)oxides can be inhibited by each other,[7] synergistic adsorption is observed more often in the co-adsorption studies.

The underlying mechanisms of the co-adsorption are rather complex and they are significantly affected by factors such as solution conditions, the nature and density of the sorbent species, and the surface structure of the selected iron (oxyhydr)oxides.[9-11] For example, arsenate and Zn(II) formed ternary complexes on goethite (Gt) surfaces at low adsorbed density, whereas they formed adamite-like surface precipitates at high density.[12] In addition, sulfate and Pb(II) primarily formed ternary complexes at low pH values and high Pb(II) concentrations, while dominant electrostatic interactions were postulated at high pH values and low Pb(II) concentrations.[13] It is worth noting that oxyanions having strong affinities to mineral's surface and complexing strongly with metals in solution often form surface ternary complexes in the co-adsorption systems. For instance, phosphate and arsenate, commonly regarded as strong ligands to the surfaces, are mostly reported to form ternary complexes or surface precipitates in the co-adsorption systems.[14-16] On the other hand, sulfate, which rarely forms ligand–metal complexes in solution, is thought to be adsorbed with heavy metal cations through electrostatic interaction and/or $\equiv FeOHMSO_4$ ternary complexes formation.[13, 17] One can speculate that the mobility of heavy metal cations could be varied in the environment enriched with different

anions due to the differences in the synergistic adsorption characteristic. However, comparison studies and discussions on the co-adsorption characteristics as related to properties of anions are insufficient.

When considering iron (oxyhydr)oxides minerals, ferrihydrite (Fh) is one of the most important geosorbents because it is ubiquitous in the environment and one of the most reactive minerals with a variety of functional groups, and has an extremely large specific surface area (> 200 m^2/g).[18-19] A number of studies suggested mechanisms for the co-adsorption of metal cations and oxyanions on Fh, but no consistent conclusion was ever reached. Swedlund et al.[20] used FITEQL simulations to propose that sulfate co-adsorbed with Co(II), Pb(II), and Cd(II) forming cation-bridged ternary complexes. A similar mechanism was proposed for the co-adsorption of Cu(II) and Pb(II) with phosphate, using extended X-ray absorption fine structure (EXAFS) and surface complexation modeling (SCM).[11] However, many studies are different from these results. Antelo et al.[16] described Fh−PO_4−Ca and Fh−AsO_4−Ca as anion-bridged ternary complexes using SCM. In our previous study, we proposed the formation of phosphate- bridged ternary complexes in the co-adsorption of phosphate and Zn(II) on Fh using X-ray photoelectron spectroscopy (XPS) and *in situ* attenuated total reflectance Fourier transform infrared spectroscopy (ATR-FTIR).[21] In addition, there are EXAFS and X-ray diffraction (XRD) measurements that support surface precipitation of arsenate and Fe(III) at the surfaces of Fh.[22-23] These discrepancies suggest that more systematic studies and discussions are necessary to gain a fundamental knowledge of the co-adsorption behaviors of metal cations and oxyanions on Fh.

At present, SCM and spectroscopy-based approaches are the main tools employed to explore the synergistic adsorption mechanisms of metal cations and oxyanions on Fh. SCM can provide guidance in predicting the reactivity of ions at mineral−water interfaces by extrapolating from data obtained in batch experiments. EXAFS spectroscopy can provide coordination numbers and bond distances of

the adsorbed ions. However, the analysis of EXAFS data is hindered by the difficulties in detecting light elements (e.g., phosphorus or sulfur),[24-26] and the necessity of analyzing multiple adsorption centers in co-adsorption systems.[27] ATR-FTIR spectroscopy can provide real-time measurement of the vibration signals of the ions that are composed of light elements.[10, 28-32] However, previous analysis of ATR-FTIR data on the adsorption of anions onto iron (oxyhydr)oxides resulted in different interpretations of the results, due to differences in experimental conditions and difficulties in analyzing the overlapped bands. Therefore, a comprehensive discussion of these results is needed to utilize the technique more effectively. Besides, methods for improving the accuracy of data analysis could be helpful. In recent years, two-dimensional correlation spectroscopy (2D-COS), has emerged as a promising technique to aid the interpretation of surface complexes and their corresponding vibrational features.[33-37] 2D-COS is also flexible and has been applied to many spectroscopies (IR, NIR, Raman, ultraviolet-visible, fluorescence, and NMR). Thus, ATR-FTIR in combination with 2D-COS is a promising method to provide valuable information for untangling the co-adsorption behaviors of metal cations and oxyanions on mineral surfaces.

In the present study, we investigated the co-adsorption of heavy metal cations and oxyanions on iron (oxyhydr)oxide minerals. Sulfate/phosphate and Cd(II) were selected as representative oxyanions and heavy metal cation, respectively, as they are common contaminants in the natural environment. In addition, as phosphate and sulfate have different complex capacities with heavy metal cations and Fh, the comparison study may provide novel information. Batch adsorption experiments and *in situ* ATR-FTIR in combination with 2D-COS were used to provide novel insight into the mechanism of the co-adsorption behaviors of Cd(II) with sulfate/phosphate on Fh and to predict the fate of heavy metal cations and oxyanions in the surficial environment.

2. Materials and methods

2.1. Materials and characterization

$Cd(NO_3)_2 \cdot 4H_2O$, NaOH, HNO_3, $Fe(NO_3)_3 \cdot 9H_2O$, NaH_2PO_4, and Na_2SO_4 of analytical grade (purity > 99%) were obtained from Guangzhou Chemical Reagent Factory. All reagents were used as received.

Fh was synthesized using a modification of the method reported by Schwertmann and Cornell.[1] A solution of $Fe(NO_3)_3$ (1 M, 50 mL) was added dropwise to a solution of NaOH (6 M, 25 mL) under vigorous magnetic stirring, until the pH of the solution was stable at 7. The resulting suspension was centrifuged at 4000 rpm, and the precipitate was washed using ultra-pure water (>18 MΩ/cm) and freeze-dried. The final product was ground to pass a 200-mesh sieve and stored at 4°C.

The X-ray diffraction (XRD) pattern of Fh was recorded using a Bruker D8 ADVANCE X-ray diffractometer (Karlsruhe, Germany), operating at 40 kV and 40 mA using CuKα radiation. The freeze-dried product showed two broad characteristic peaks of 2-line Fh (Figure S1). The specific surface area was measured to be 309 m^2/g using a Surface Area & Pore Size Analyzer from Quantachrome. This value is consistent with previous data.[11]

2.2. Batch adsorption/desorption experiments

Co-adsorption of Cd(II) with sulfate or phosphate was investigated using batch experiments. All batch experiments were carried out by adding 0.05 g of Fh to 20 mL 1 mM $NaNO_3$ solution (solid concentration was 2.5 g/L) containing different concentrations of Cd(II) and oxyanions. The reactions occurred in 50 mL polypropylene bottles while they were vigorously shaken in an orbital shaker at 150 rpm 25°C. These included adsorption isotherms and pH adsorption edges. Adsorption isotherms were measured using initial concentrations of 0.2–2 mM of Cd(II) on Fh, in the absence or presence of 0.5, 1, or 2 mM of oxyanions (i.e., sulfate or phosphate) at an initial solution pH 5. The pH adsorption edges were measured with initial concentrations of 0.5, 1, or 2 mM of oxyanions, and 0.2

mM of Cd(II); hereafter these systems are referred to as 0.5S/P+Cd, 1S/P+Cd, or 2S/P+Cd, respectively.

Desorption of Cd(II) and oxyanions was conducted by removing the supernatant after the adsorption equilibrium was reached, replacing with an equal volume of 0.3 M NaCl solution at pH 5, and stirring the sample for 24 h. Finally, the concentrations of Cd(II) and oxyanions in the supernatant were determined after desorption. Four points were chosen from the adsorption isotherms: 1S+Cd, 2S+Cd, 1P+Cd, and 2P+Cd, in which the initial concentrations of oxyanions were 1 or 2 mM, and the concentration of Cd(II) was 2 mM. The molar ratio of Cd/(S or P) can therefore be 2 or 1.

After the reactions reached equilibrium, the polypropylene bottles were centrifuged at 4000 rpm for 10 min, and then the upper layer suspension was filtered through 0.45 μm filter membrane to obtain the supernatant for further analysis. The concentration of Cd(II) was determined by atomic absorption spectroscopy (Perkin Elmer AAnalyst 400, USA). The concentration of phosphate was determined by UV-VIS spectrophotometry,[38] and the concentration of sulfate was determined using high performance anion exchange chromatography (Dionex ICS 900, USA).

Simulation of ion speciation in equilibrium solutions, and the saturation index values of the potential Cd solid phases were calculated using visual MINTEQ (version 3.0, John Gustafsson, KTH, Sweden). The distribution of Cd(II) and ligand species in 1 mM $NaNO_3$ solution was calculated based on the total soluble Cd(II) and oxyanions concentration, at fixed pH values and CO_2 partial pressure of 0.00038 atm (~38.5 Pa) at 25°C.

2.3. *In situ* ATR-FTIR spectroscopy

In situ ATR-FTIR measurements were conducted using a Bruker Vertex-70 FTIR spectrophotometer, equipped with a multi-bounce horizontal ATR accessory and flow cell (Pike Technologies). A horizontal ZnSe ATR crystal was coated with a film of Fh (2.5 mg) by drying Fh

suspension. The solution pH was monitored throughout the experiment and adjusted by adding small amounts of 0.5 M HCl or 0.5 M NaOH. The Fh deposit was allowed to equilibrate with the background solution (1 mM NaCl), after which a spectrum was collected as a background. The adsorption experiments were conducted with different solutions of Cd(II) and oxyanions circulated through a peristaltic pump at a rate of 1 mL/min. The concentrations of anions and Cd(II) were 100 and 50 μM, respectively. All of the spectra were collected at 25°C over a range of 400–4000 cm^{-1}, with a resolution of 4 cm^{-1} and 64 scans. The Fh film was checked at the end of each adsorption experiment, and no erosion of the film was observed. The spectra were baseline corrected before analysis following previously published procedures [28, 37].

2.4. Analysis of ATR-FTIR data

Analysis of ATR-FTIR data was based on the symmetry argument,[13] which assigns molecular symmetry based on the number and position of peaks. A free tetrahedral anion has tetrahedral symmetry and belongs to the point group T_d; this has only one triply degenerate v_3 band. Adsorption of tetrahedral oxyanions (e.g., sulfate and phosphate) to minerals' surfaces (e.g., iron (oxyhydr)oxides) leads to symmetry reduction from T_d to C_{3v}, C_{2v}, or C_1, with the triply degenerate v_3 band splitting into two, three, or three v_3 bands. The relationship between the number of active bands and the symmetry of the anions has been successfully applied to interpret the bonding configurations of anions at mineral surfaces.[13, 17] To better examine the changes of the overlapped bands, several spectra at equal time intervals were selected for 2D-COS analysis proposed by Noda,[34] using the software "2D Shige" released by Shigeaki Mortia (Kwansei-Gakuin University, Japan). Synchronous and asynchronous spectra can be obtained from this analysis. In the synchronous spectra, auto peaks are responsible for the changes of peak intensity over time, while cross peaks provide the responses of two different bands to a time perturbation. In asynchronous spectra, only cross peaks are present. This

indicates the uncorrelated response of two bands, likely originating from different surface complexes. Therefore, the resolution of highly overlapped peaks can be greatly enhanced, and the assignments of peaks belonging to each species can be facilitated by 2D-COS analysis.

3. Results and discussion

3.1. Batch adsorption/desorption experiments

Adsorption of Cd(II) on Fh in the absence of oxyanions was found to be weak, with an adsorbed amount of 0.04 mmol/g at initial Cd(II) concentration of 2 mM (Figure 1A). The adsorption of Cd(II) resulted in a small decrease of solution pH from ~ 5 to 4.8. In the presence of phosphate and sulfate, the adsorbed Cd(II) increased to ~0.33 mmol/g (0.5 mM oxyanions) and ~0.36 mmol/g (1 mM oxyanions), respectively. As the concentration of oxyanions increased to 2 mM, the differences in co-adsorption of Cd(II) with phosphate or sulfate on Fh became more pronounced, with an adsorbed amounts of Cd(II) of 0.55 and 0.45 mmol/g in the presence of phosphate and sulfate, respectively.

Oxyanions were removed from solution completely at concentrations of 0.5 and 1 mM, but not at higher concentration (2 mM). At this high concentration of oxyanions, the adsorbed amounts of phosphate were slightly larger than those of sulfate (Table S1), indicating a different co-adsorption capacity towards Cd(II) on Fh. The adsorption of phosphate and sulfate increased the solution pH (from ~5 to ~6–7.5) at low concentrations of Cd(II), whereas only weak changes of the solution pH (±0.2) were observed at higher concentrations of Cd(II). The change in solution pH after the adsorption suggests a ligand exchange process.

The desorption of Cd(II) and oxyanions at pH 5 in P+Cd and S+Cd systems are different (Figure 1B). The desorbed percentages of Cd(II) in P+Cd systems were smaller than those in S+Cd systems. The desorbed Cd(II) decreased with increasing concentration of phosphate, and barely any phosphate ions were detected in the supernatant after the desorption reached equilibrium. As reported in previous

studies,[39-41] strong ligands such as phosphate and arsenate do not get replaced by electrolytes such as NaCl and $NaNO_3$. Unlike P+Cd systems, desorbed percentages of both Cd(II) and sulfate increased with increasing concentration of sulfate in S+Cd system. The desorption of Cd(II) was not accompanied by the desorption of phosphate in P+Cd systems, indicating a stronger affinity of Fh surface for phosphate compared to Cd(II). Negligible changes of the solution pH (±0.1) were observed after the desorption equilibrium. The differences in the desorption of Cd(II) and oxyanions in P+Cd and S+Cd systems indicate different mechanisms of co-adsorption, and reveal the different capacity of phosphate and sulfate ions in the long-term immobilization of Cd(II) on Fh.

3.2 pH adsorption edges and thermodynamic calculations

As shown in the pH adsorption edges (Figure 2A), the percentage of adsorbed Cd(II) increased with increasing solution pH, from ~0% at pH 3 to ~100% at pH 8. The pH at which 50% of the Cd(II) was adsorbed (pH_{50}) was ~5. In the presence of 0.5 mM oxyanions, the adsorption edge shifted to lower pH with the pH_{50} decreased by nearly 1 pH unit (from 5 to 4). Little difference was observed between sulfate and phosphate in affecting the adsorption edges of Cd(II) at this concentration. At oxyanion concentrations of 1 mM, adsorption of Cd(II) in the S+Cd system was slightly more pronounced as compared to that in the P+Cd system. As the concentration of oxyanions further increased to 2 mM, the adsorption of Cd(II) in the P+Cd system was more pronounced than it was in the S+Cd system in the pH range of 3–5. The calculated saturation index (Figure S2) of potential Cd solid phases (e.g., $Cd(OH)_2$ and/or $Cd_3(PO_4)_2$) was < 0 in the pH range of the experiments (pH 4–8 for Cd system and pH 3–6 for Cd+ligands systems). Thus, as precipitation of Cd solid phases in solution can be ruled out, the removal of Cd(II) from solution can be assigned entirely to Fh.

Based on the available thermodynamic data, the speciation diagrams of Cd(II) in the presence of phosphate or sulfate were calculated using visual MINTEQ (Figure 2B and C). In S+Cd systems,

Cd^{2+} was the predominant species, with a small fraction of $CdSO_4$(aq) co-existing at pH from 3 to 8. As the concentration of sulfate increased from 1 to 2 mM, the concentration of Cd^{2+} decreased, while that of $CdSO_4$ (aq) increased. In contrast, the distribution of species of Cd(II) in P+Cd systems was highly dependent on solution pH. At phosphate concentration of 1 mM, Cd^{2+} and $CdHPO_4$(aq) were the dominant species at solution pH<6.8 and pH > 6.8, respectively; This threshold shifted to pH 6.3 at phosphate concentration of 2 mM. It should be noted that at solution pH < 4, the species of Cd(II) in Cd+P systems were unchanged with the change of phosphate concentration; thus, the shift of pH edge from 3.5 to 2.6 with the concentration of phosphate increased from 1 to 2 mM was irrelevant to the soluble metal-ligand complexes, i.e., $CdHPO_4$(aq).

3.3. Infrared spectroscopy results

3.3.1 Sulfate/Fh spectra in the absence or presence of Cd(II)

Adsorbed sulfate on Fh displayed asymmetric bands in the IR spectrum (Figure 3A), unlike sulfate in solution that showed symmetric bands centered at ~1100 cm^{-1} (Figure S3). The synchronous contour plots (Figure 3B) exhibit only one prominent auto peak on the diagonal at ~1100 cm^{-1}, indicating a strong change in the intensity of the peak. The asynchronous spectra show four peaks at 1155, 1140, 1100, and 1048 cm^{-1}, and the peak at ~1100 cm^{-1} has asynchronous signal with the other three peaks. Thus, two sets of peaks for sulfate spectra at pH 7 and 5 can be distinguished. The adsorption of sulfate at pH 9 was too weak to obtain a 2D contour plot. Details of 2D data analysis are summarized in Table S2. The peak at 1100 cm^{-1} represents the outer-sphere complexes of sulfate. Another species with two distinctive peaks at 1048 and 1140 cm^{-1} and a shoulder at 1155 cm^{-1} can be considered as bidentate inner-sphere sulfate complexes, similar to the species proposed by Zhang et al.[31] As the adsorption of sulfate increased with decreasing pH, the ν_1 band became more prominent, although sulfate ions were adsorbed as both outer and inner-sphere complexes at pH 7. The curve-

fitting results (Figure S4) suggest that the proportion of inner-sphere surface complexes increased from ~33% to 40% (estimated from the area of the peaks) as the solution pH decreased from 7 to 5. It is worth noting that sulfate is adsorbed only as inner-sphere surface complexes on hematite (Hm),[42-43] while it forms a mixture of outer and inner-sphere complexes on Gt at pH ≤ 6.[28] while on Fh, a mixture of the two complexes can form at pH ≤ 7. This adsorption behavior of sulfate on Fh is similar to Gt where a mixture of outer and inner-sphere surface complexes is found at pH values up to 7. This result indicates the different adsorption reactivity of the three iron (oxyhydr)oxides towards sulfate.

With the co-existence of Cd(II), the IR spectra of sulfate became broader (Figure 3C), particularly at higher solution pH (7 and 9), indicating a more complicated split of IR active bands. The multiple signals exhibited in the 2D asynchronous spectra (Figure 3D) further verify the complicated split. Thus, Cd(II) not only promoted sulfate adsorption, but also generated a more diverse co-adsorption environment with three species co-existed on the surfaces of Fh (Table 1and details in Table S3). At pH 9, large amounts of sulfate (~51%) were adsorbed as outer-sphere complexes, with the presence of both C_{2v} or C_1 inner-sphere complexes, in addition to the inner-sphere complexes with bands at 1085 and 1020 cm^{-1}. As the pH decreased (to pH 7 and 5), the same three complexes co-existed on Fh with the proportion of outer-sphere complexes decreasing (40% and 36%, respectively) and that of the inner-sphere complexes increasing, similar to the results of sulfate adsorption. The proportions of C_{2v} inner-sphere complexes in the co-adsorption systems (~38% at pH 7 and 41% at pH 5) were larger than those in the single systems (~31% at pH 7 and 35% at pH 5).

The increase of proportion of inner-sphere complexes can correspond to two scenarios. In the first scenario, the inner-sphere complexes are adsorbed on Fh; while the negative sulfate anions can reduce the surface charge of Fh thus enhancing the attraction between the surface and Cd(II), the

adsorbed Cd(II) can increase the proportion of inner-sphere sulfate complexes in a similar way. In the second scenario, a part of sulfate is adsorbed directly to Cd(II). Sulfate and Cd(II) can be adsorbed synergistically, but they can still compete for Fh surface sites. Hence, the proportion of outer-sphere complexes would decrease, and sulfate would interact with the adsorbed Cd(II) forming ternary complexes with a C_{2v} symmetry. As Cd(II) ions are multi-coordinated in an aqueous environment, this could also involve sulfate. However, if the sulfate was directly bound to Cd(II), the change of bonding environment should cause an evident shift of the bands, which was not detected in this study. Therefore, the increased formation of inner-sphere complexes could be primarily due to the surface charge modification induced by Cd(II) on Fh, hence the first scenario.

The additional surface complexes seen in S+Cd systems (as compared with single adsorption systems) showed two bands at 1085 and ~1030 cm^{-1}. In the co-adsorption study of Cd(II) and sulfate on Gt,[31] complexes with bands at 1115 and 1080 cm^{-1} were identified as ternary complexes with monodentate-like symmetry (C_{3v}). A shoulder at 1025 cm^{-1} was also distinguished in their difference spectra, although this was not taken into account. These results are quite similar to the bands observed in our study on Fh. Therefore, the band at 1130 cm^{-1}, which had no asynchronous signal with the bands at 1085 and 1020 cm^{-1}, could be a shared band between two species; this will also explain the relative high intensity of the band at 1130 cm^{-1} in the S+Cd system. Besides, the overestimation to the peak area of the complexes with C_{2v} symmetry should be considered, but overrating to a single band cannot cause an increase to ~6% of the corresponding complexes. As the shoulder band at 1020 cm^{-1} was extremely weak, the surface complexes could be assigned as monodentate-like complexes with C_{3v} symmetry.[31] It is possible that the peak at 1020 cm^{-1} could be the result of a hydrogen bond between an oxygen atom of a monodentate complexes and an adjacent surface site. Two possible configurations can be proposed based on this argument (Figure 4). Cd(II) can be coordinated in a

297 bidentate binuclear fashion to Fe-OH or S-OH, as suggested by the EXAFS results in previous
298 studies.[44] In configuration A (Figure 4A), monodentate inner-sphere sulfate surface complexes have
299 an additional hydrogen bond to the adjacent adsorbed Cd(II). In configuration B (Figure 4B), sulfate
300 coordinates to adsorbed Cd(II) with an additional hydrogen bond to the adjacent water molecules,
301 forming cation-bridged ternary complexes.

302 To further evaluate the co-adsorption mechanism of sulfate and Cd(II), the quantity of Fh surface
303 sites was calculated using a Gran plot (Figure S5) to be ~2.78 sites/nm^2, and the available adsorption
304 sites were ~6.04×10^{20} sites/g. The concentrations of Cd(II) and sulfate were also monitored before
305 and after the *in situ* adsorption experiment, and the estimated total adsorbed amounts of Cd(II) and
306 sulfate were no less than 8.00×10^{20} ions/g in all systems. Considering the potential steric hindrance
307 of the adsorbed species and the occupation of surface sites by bidentate species, the surface sites were
308 insufficient for monolayer adsorption of the ions in S+Cd systems. Hence, surface precipitation and/or
309 ternary complexes (configuration B) should be included in the analysis. However, as the IR spectrum
310 of $CdSO_4(s)$[31] has sharp peaks at 1111, 1095 cm^{-1} and a weak peak at 978 cm^{-1}, which were not seen
311 in our IR spectra, surface precipitation can be excluded. The synergistic adsorption of sulfate and
312 Cd(II) could be attributed to the change in Fh surface charge, as proved by the increase of inner-
313 sphere C_{2v} sulfate complexes in the presence of Cd(II), and to the adsorbed Cd(II) that can bond
314 sulfate forming ternary complexes. Moreover, we have observed a high desorption rate of sulfate in
315 macroscopic studies, which suggests that the presence of monodentate sulfate as part of ternary inner-
316 sphere complexes is relatively unstable. This instability has also been proposed for chromate surface
317 complexes on Fh.[45]

318 ### 3.3.2 Phosphate/Fh spectra in the absence or presence of Cd(II)

319 Multiple bands of the adsorbed phosphate are seen in both synchronous and asynchronous

contour plots (Figure 5B), indicating that there is a more complicated correlation between the peaks and thus there could be a variety of phosphate surface complexes. In the phosphate adsorption systems, three bands at 1075, 1025, and 950 cm^{-1} are seen in the asynchronous spectra at pH 9, which can be identified as bidentate non-protonated inner-sphere complexes; this was also seen previously on Gt[46-47] and Fh.[29] At pH 7 (details in table S4), two sets of bands are identified. Whereas the fraction of bidentate non-protonated inner-sphere complexes decreased (~69%), outer-sphere surface complexes with C_{3v} symmetry (1100 and 970 cm^{-1}) were observed. As these bands are close to those of HPO_4^{2-}(aq) (Figure S6), this indicates the formation of outer-sphere surface complexes of HPO_4^{2-} via electrostatic attraction and/or hydrogen-bonding complexes. At solution pH 5, the proportion of the bidentate non-protonated inner-sphere complexes further decreased (~57%), and complexes with C_{2v} symmetry were detected.

The synchronous spectra of phosphate in the presence of Cd(II) are similar to those in the absence of Cd(II), but asynchronous contour plots show evident differences. At lower solution pH (5 and 7), at least three phosphate complexes co-existed on the surfaces of Fh (Table 2). This will be discussed in details in the next section. At pH 9, two sets of bands can be identified (Figure 5D): complexes with peaks at 1090, 1033, and 936 cm^{-1}, and complexes with peaks at 1118, 1070, and 975 cm^{-1}. The former set is attributed to bidentate non-protonated inner-sphere complexes as in the single adsorption system at pH 9. The band at 1118 cm^{-1} of the latter set is consistent with the ν(P=O) vibration, which is found only at lower pH when bidentate mono-protonated phosphate complexes are formed, as reported in previous studies.[30, 46] This band suggested the formation of two different complexes (Figure 6). In configuration A, P-bridged ternary complexes are formed, whereas in configuration B, protonated monodentate phosphate complexes are adsorbed on the surface of Fh, with additional bonding to the adjacent adsorbed Cd(II). To determine the most likely configuration,

the concentrations of Cd(II) and phosphate before and after the adsorption were measured. The total adsorbed amounts of Cd(II) and phosphate ($\geq 8.02\times10^{20}$ ions/g) were greater than the available surface sites as reported in section 3.3.1, suggesting the formation of ternary complexes and/or surface precipitation. However, surface precipitation can be excluded, since the adsorption isotherms are quite different from the model of surface precipitation proposed by Farley et al;[48] besides, the difference spectra (spectra of co-adsorption systems minus those of single adsorption systems) (Figure S8) show a significant difference compared to the reference spectra of Cd−PO_4 precipitates [10]. Thus, we propose that Fe−P−Cd ternary complexes (configuration A) should be the most likely complexes that form as the newly generated species in the co-adsorption systems.

3.4 Discussion and comparison with previous work

Many studies have demonstrated that sulfate and phosphate could be adsorbed synergistically with heavy metal cations by iron (oxyhydr)oxides.[20, 39, 49-51] Most of the studies on co-adsorption of sulfate and Cd(II) on Gt and Fh reported a shift of pH_{50} between 0.4−0.8 of the Cd(II) adsorption edge (Table 3),[20, 49, 51] whereas a shift of 1-2 was found in this study. This discrepancy is related to the properties and dosages of adsorbents, the ionic strength, and the concentrations of sulfate and Cd(II). As shown in Table 3, systems with lower ionic strength show a more significant shift of the Cd(II) adsorption edge. This dependence is consistent with the formation of Cd-bridged ternary complexes. As pointed out by Hoins et al.[51] in model calculation studies on Gt, co-adsorption of anions and cations accompanied by the formation of cation-bridged ternary complexes can be inhibited by high ionic strength due to charge repulsion. In contrast to the results in S+Cd systems, the pH_{50} of Cd(II) shifted to lower pH by 1.2−2 units in the presence of phosphate as reported in previous[39, 50] and the present studies, although at different ionic strengths. Comparison with previous literature suggests that the co-adsorption of sulfate and Cd(II) decreases in solutions with higher ionic

strength, whereas the co-adsorption of phosphate and Cd(II) is much less sensitive to ionic strength.[20, 39, 49-51] Therefore, comparative experiments carried out under the same conditions are essential in verifying the differences between Cd+S and Cd+P co-adsorption systems.

Although a large number of studies deal with ATR-FTIR characterization of sulfate and phosphate complexes forming at iron (oxyhydr)oxide surfaces, the results and assignments are varied. One general standpoint is that sulfate is only adsorbed as inner-sphere complexes on Hm, and as a mixture of outer and inner-sphere complexes on Gt and Fh when the pH is below the point of zero charge. This difference can be attributed to the differences in surface physicochemical properties of the minerals (i.e., surface charge). In addition, the density and topology of surface functional groups can also contribute to different adsorption behavior as discussed by Peak et al.[28] When inner-sphere complexes are assigned to IR active bands, the results are not always consistent. Hug et al.[43] proposed that when sulfate was adsorbed on Hm, it was predominantly adsorbed as monodentate complexes with two ν_3 bands (1128 and 1059 cm^{-1}). The weak shoulder band at 1185 cm^{-1} in the IR spectra was attributed to hydrogen-bonding interactions between sulfate and adjacent water molecules of the iron hydration shell. Peak et al.[28] and Wijnja et al.[52] suggested that there was a combination of outer-sphere and inner-sphere sulfate complexes on Gt based on their assignment of the peaks of inner-sphere complexes at 1043, 1121, and 1175 cm^{-1} and that of outer-sphere complexes at 1105 cm^{-1}. Peak et al.[28] further proved that the inner-sphere complexes were either monodentate bisulfate surface complexes or monodentate sulfate surface complexes with hydrogen bonding to an adjacent surface site by using D_2O as a solvent. In contrast, Lefevre and Fédoroff[53] proposed the possibility that there was a mixture of monodentate and bidentate complexes, with the calculations of Paul et al.[54] supporting this standpoint. Recent studies of Zhu et al.[55] and Gu et al.[56] confirmed the formation of bidentate binuclear inner-sphere and outer-sphere complexes on Fh surfaces, based on the three ν_3

389 bands (1043, 1121, and 1175 cm^{-1}) of ATR-FTIR spectra, in combination with the results of EXAFS
390 and quantum mechanical calculations.

391 The different interpretation of the ATR-FTIR data in these studies could be due to the differences
392 in the FTIR techniques (most notably the use of in situ versus ex-situ conditions during data
393 collection), reaction conditions (e.g., anions/adsorbent ratios), quantity and reactivity of sites on the
394 minerals, and the complexity of surface species (i.e., multiple complexes may exist simultaneously).
395 The two complexes assigned respectively by Peak et al.[28] and Zhu et al.[55] to the species with bands
396 at 1043, 1121, and 1175 cm^{-1} could form on the minerals simultaneously, but their relative amounts
397 can vary due to the differences of site densities and reactivity on Gt and Fh. The results of our *in situ*
398 ATR-FTIR study in single adsorption systems were consistent with that of Zhu et al.;[55] thus we can
399 state that bidentate binuclear complexes are the dominant inner-sphere sulfate complexes on Fh,
400 accompanied by the outer-sphere complexes.

401 In the presence of divalent cations, Swedlund et al.[20, 49] proposed the formation of ≡$FeOHMeSO_4$
402 ternary complexes with heavy metal cations (Co(II), Pb(II), and Cd(II)) directly bonding to Fh, based
403 on the diffuse layer modeling results. Zhang et al.[31] concluded that the additional sulfate complexes
404 in the co-adsorption systems with bands at 1115 and 1080 cm^{-1} were ternary complexes with
405 monodentate-like symmetry (C_{3v}) on Gt. They also suggested that a portion of the initially adsorbed
406 inner-sphere complexes were converted into Cd-SO_4 ternary complexes with the addition of Cd(II).
407 In contrast, an increased proportion of the initial inner-sphere complexes was observed in this study.
408 As discussed above, the electrostatic attraction combined with the formation of cation-bridged ternary
409 complexes, contributed to the synergistic adsorption, which is also in agreement with the batch
410 adsorption and desorption experiment and spectroscopic results. This difference is a consequence of
411 the higher surface area and more abundant functional groups on Fh compared to Gt. Considering the

amorphous structure of Fh and the diversity of its surface sites, topology, and reactivity, it is likely that different mechanisms contributed to the synergistic adsorption of oxyanions and Cd(II).

Elzinga and Sparks[30] discussed the adsorption of phosphate on iron (oxyhydr)oxides, with focus on three complexes. The first complexes are preferentially formed on Hm at low pH and high surface coverage in the pH range 3.5–7.5, and show IR bands at 1117, 1007, and 964 cm^{-1}. The second complexes have three bands at 1086, 1034 and 966 cm^{-1} and are assigned as a bridging non-protonated surface complexes. The third complexes forming at pH values above 6, have two bands at 1057 and 966, or 1075 and 990 cm^{-1} depending on the adsorbent, and they are assigned as monodentate mononuclear non-protonated surface complexes. The phosphate adsorption on different iron (oxyhydr)oxides produced different results; as mentioned above, this should be due to the surface properties of the minerals. For example, phosphate complexes at Fh surfaces at high pH (e.g., 7.5) are non-protonated, whereas protonated phosphate complexes form at Hm surface under similar condition.

In this study, C_{2v} complexes formed at Fh surfaces in all the adsorption systems are consistent with bridging non-protonated surface complex. The C_{3v} complexes formed at pH 7 with two peaks at ~1100 and 970 cm^{-1}, are likely to be outer-sphere or hydrogen-bonded surface complexes, as explained above. We also detected C_{2v} complexes at pH 5, which are generally found at pH<7.5 in previous studies.[29-30]. As their bands (1105, 1050, and 995 cm^{-1}) are fairly similar to that of the monodentate mononuclear Fe–P (aq) complexes reported by Arai et al.,[29] we are able to assign them as protonated monodentate complexes. As the loading of phosphate was comparatively high at low pH, it is likely that this will form monodentate complexes due to the lack of surface sites and steric hindrance.

In the co-adsorption systems, slight differences in the band positions between the C_{2v} complexes

formed at high pH (with bands at 1090, 1033, and 936 cm^{-1}) and those formed at low pH (with bands at 1080, 1045, 935 cm^{-1}) were observed. Similar results were reported by Elzinga and Kretzschmar[10] in the co-adsorption of phosphate and Cd(II) onto Hm. They proposed that Cd-bridged complexes should be the dominant species at high pH, and phosphate-bridged complexes became dominant at low pH. However, they also suggested that their IR data could not rule out the possibility of differences in the phosphate protonation state. The C_{3v} complexes at pH 7 can be assigned to monodentate mononuclear non-protonated complex as was also proposed by Persson.[47] The C_{3v} complexes at pH 5, however, should be outer-sphere surface complexes of HPO_4^{2-} formed via electrostatic attraction and/or hydrogen-bonding complexes. In comparison with the spectra of phosphate at pH 5 in the single adsorption system, the extra C_{3v} complexes suggest that electrostatic interactions could also have contributed to the synergistic adsorption of phosphate and Cd(II). Still, the species with a band of *v*(P=O) could be detected in all the co-adsorption systems, indicating the presence of species with similar symmetry.

Antelo et al.[16] found that Fh−PO_4−Ca ternary complexes could be adequately described by the CD model based on the experiment data. However, Tiberg et al.[39] identified a Cd···P distance at approximately 3.4 Å by EXAFS analysis, indicating the formation of ternary complexes, and then proposed the formation of Fe−Cd−P ternary complexes on Fh based on the obtained distances of Cd-O, Cd···Fe, Cd···P and SCM results. Contrary to Tiberg's interpretation, we propose the presence of Fe−P−Cd ternary complexes based on the appearance of the *v*(P=O) band in the co-adsorption systems, similar to that reported by Hinkle et al.[57] in their studies on co-adsorption of Fe(II) and phosphate on Gt and Hm. As EXAFS provides only average structural information over a short-range near 5 Å, and the distance of Fe···Cd could be larger than 6.5 Å in the Fe−P−Cd ternary complexes, the evidence of Fe−P−Cd ternary complexes could be overlooked by EXAFS analysis. Singh et al.[58]

also suggested in their co-adsorption study of uranium and phosphate on Gt that while their EXAFS data could be explained by U-bridging ternary surface complexes, it was impossible to statistically distinguish this scenario from that of P-bridged complexes. Hence, we propose that phosphate-bridged ternary complexes can also form in the co-adsorption of phosphate and Cd(II) on Fh; the electrostatic interaction should have made a contribution at the same time.

Conclusions

This study confirms that Cd(II) was adsorbed synergistically with sulfate and phosphate on Fh. Sulfate and phosphate at low concentrations (0.5 or 1 mM) showed a similar synergistic adsorption capacity to Cd(II). However, it is striking that the efficiency of phosphate was enhanced at high anion concentrations (2 mM) with a greater uptake of Cd(II). In addition, the percentages of desorbed Cd(II) and oxyanions in P+Cd systems were smaller than those in S+Cd systems, indicating a stronger long-term immobilization of phosphate and Cd(II) when they are co-existed. The results of ATR-FTIR spectroscopy indicated that the synergistic adsorption of sulfate and Cd(II) was due to electrostatic interaction and the formation of cation-bridged ternary complexes. In contrast, phosphate form anion-bridged ternary complexes with Cd(II) in most of the co-adsorption systems, in addition to the electrostatic interaction. Thus, this study provides additional insights for understanding the geochemical processes involving heavy metal cations and naturally occurring ligands.

Acknowledgements

This work was supported by the National Key Research and Development Plan of China (2016YFD0800700), the National Natural Science Foundation of China (41572031), the Newton Advanced Fellowship (NA150190), the National Program for Support of Top-notch Young Professionals, and the Guangdong Provincial Youth Top-notch Talent Support Program (2014TQ01Z249).

References

1. Schwertmann, U.; Cornell, R. M. Iron Oxides in the Laboratory: Preparation and Characterization. VCH: Weinheim, Germany, **1991**.
2. Madden, A. S.; Hochella, M. F.; Luxton, T. P. Insights for Size-dependent Reactivity of Hematite Nanomineral Surfaces through Cu^{2+} Sorption. *Geochimica et Cosmochimica Acta*, **2006**, 70, 4095–4104.
3. Ponthieu, M.; Juillot, F.; Hiemstra, T.; van Riemsdijk, W. H.; Benedetti, M. F. Metal Ion Binding to Iron Oxides. *Geochimica et Cosmochimica Acta*, **2006**, 70, 2679–2698.
4. Kim, J.; Li, W.; Philips, B. L.; Grey, C. P. Phosphate Adsorption on the Iron Oxyhydroxides Goethite (alpha-FeOOH), Akaganeite (beta-FeOOH), and Lepidocrocite (gamma-FeOOH): A P-31 NMR Study. *Energy & Environmental Science*, **2011**, 4, 4298–4305.
5. Kersten, M. and Vlasova, N. Silicate adsorption by goethite at elevated temperatures. *Chemical Geology*, **2009**, 262, 336–343.
6. Ding, X. B.; Song, X. W.; Boily, J. F. Identification of Fluoride and Phosphate Binding Sites at FeOOH Surfaces. *Journal of Physical Chemistry C*, **2012**, 116, 21939–21947.
7. Benjamin, M. M. and Leckie, J. O. Effect of Complexation by Cl, SO_4, and S_2O_3 on Adsorption Behavior of Cd on Oxide Surfaces. *Environmental Science & Technology*, **1982**, 16, 162–170.
8. Zhu, R.; Li, M.; Ge, F.; Xu, Y.; Zhu, J.; He, H. Co-sorption of Cd and phosphate on the surface of a synthetic hydroxyiron-montmorillonite complex. *Clays and Clay Minerals*, **2014**, 62, 79–88.
9. Ostergren, J. D.; Brown, G. E.; Parks, G. A.; Persson, P. Inorganic Ligand Effects on Pb(II) Sorption to Goethite (alpha-FeOOH)-II. Sulfate. *Journal of Colloid and Interface Science*, **2000**, 225, 483–493.
10. Elzinga, E. J. and Kretzschmar, R. *In situ* ATR-FTIR Spectroscopic Analysis of the Co-adsorption of Orthophosphate and Cd(II) onto Hematite. *Geochimica et Cosmochimica Acta*, **2013**, 117, 53–64.
11. Tiberg, C.; Sjostedt, C.; Persson, I.; Gustafsson, J. P. Phosphate Effects on Copper(II) and Lead(II) Sorption to Ferrihydrite. *Geochimica et Cosmochimica Acta*, **2013**, 120, 140–157.
12. Gräfe, M. and Sparks, D. L. Kinetics of Zinc and Arsenate Co-sorption at the Goethite–Water Interface. *Geochimica et Cosmochimica Acta*, **2005**, 69, 4573–4595.
13. Elzinga, E. J.; Peak, D.; Sparks, D. L. Spectroscopic Studies of Pb(II)-Sulfate Interactions at the Goethite-Water Interface. *Geochimica et Cosmochimica Acta*, **2001**, 65, 2219–2230.
14. Ler, A. and Stanforth R. Evidence for Surface Precipitation of Phosphate on Goethite. *Environmental Science & Technology*, **2003**, 37, 2694–2700.
15. Jiang, W.; Lv, J. T.; Luo, L.; Yang, K.; Lin, Y. F.; Hu, F. B.; Zhang, J.; Zhang, S. Z. Arsenate and Cadmium Co-adsorption and Co-precipitation on Goethite. *Journal of Hazardous Materials*, **2013**, 262, 55–63.
16. Antelo, J.; Arce, F.; Fiol, S. Arsenate and Phosphate Adsorption on Ferrihydrite Nanoparticles. Synergetic Interaction with Calcium Ions. *Chemical Geology*, **2015**, 410, 53–62.
17. Beattie, D. A.; Chapelet, J. K.; Grafe, M.; Skinner, W. M.; Smith, E. *In Situ* ATR FTIR Studies of SO_4 Adsorption on Goethite in the Presence of Copper Ions. *Environmental Science & Technology*, **2008**, 42, 9191–9196.
18. Zachara, J. M.; Girvin, D. C.; Schmidt, R. L.; Resch, C. T. Chromate Adsorption on Amorphous Iron Oxyhydroxide in the Presence of Major Groundwater Ions. *Environmental Science & Technology*, **1987**, 21, 589–594.
19. Swedlund, P. J. and Webster, J. G. Adsorption and Polymerisation of Silicic Acid on Ferrihydrite, and its Effect on Arsenic Adsorption. *Water Research*, **1999**, 33, 3413–3422.
20. Swedlund, P. J.; Webster, J. G.; Miskelly, G. M. The Effect of SO_4 on the Ferrihydrite Adsorption of Co, Pb and Cd: Ternary Complexes and Site Heterogeneity. *Applied Geochemistry*, **2003**, 18, 1671–1689.
21. Liu, J.; Zhu, R.; Xu, T.; Xu, Y.; Ge, F.; Xi, Y.; Zhu, J.; He, H. Co-adsorption of Phosphate and Zinc(II) on the

528 Surface of Ferrihydrite. *Chemosphere*, **2016**, 144, 1148–55.
529 22. Jia, Y. F.; Xu, L. Y.; Fang, Z.; Demopoulos, G. P. Observation of Surface Precipitation of Arsenate on
530 Ferrihydrite. *Environmental Science & Technology*, **2006**, 40, 3248–3253.
531 23. Jiang, X. L.; Peng, C. J.; Fu, D.; Chen, Z.; Shen, L.; Li, Q. B.; Ouyang, T.; Wang, Y. P. Removal of Arsenate
532 by Ferrihydrite via Surface Complexation and Surface Precipitation. *Applied Surface Science*, **2015**, 353, 1087–
533 1094.
534 24. Li, W.; Livi, K. J.; Xu, W.; Siebecker, M. G.; Wang, Y.; Phillips, B. L.; Sparks, D. L. Formation of crystalline
535 Zn–Al layered double hydroxide precipitates on γ-alumina: the role of mineral dissolution. *Environmental Science*
536 *& Technology*, **2012**, 46, 11670–11677.
537 25. Gückel, K.; Rossberg, A.; Brendler, V.; Foerstendorf, H. Binary and ternary surface complexes of U (VI) on
538 the gibbsite/water interface studied by vibrational and EXAFS spectroscopy. *Chemical Geology*, **2012**, 326, 27–35.
539 26. Manceau, A.; Lanson, B.; Schlegel, M. L.; Harge, J. C.; Musso, M.; Eybert-Berard, L.; Hazemann, J. L.;
540 Chateigner, D.; Lamble, G. M. Quantitative Zn Speciation in Smelter-contaminated Soils by EXAFS Spectroscopy.
541 *American Journal of Science*, **2000**, 300, 289–343.
542 27. Sheals, J.; Granstrom, M.; Sjoberg, S.; Persson, P. Co-adsorption of Cu(II) and Glyphosate at the Water-
543 goethite (alpha-FeOOH) Interface: Molecular Structures from FTIR and EXAFS Measurements. *Journal of Colloid*
544 *and Interface Science*, **2003**, 262, 38–47.
545 28. Peak, D.; Ford, R. G.; Sparks, D. L. An *in situ* ATR-FTIR Investigation of Sulfate Bonding Mechanisms on
546 Goethite. *Journal of Colloid and Interface Science*, **1999**, 218, 289–299.
547 29. Arai, Y. and Sparks, D. L. ATR–FTIR Spectroscopic Investigation on Phosphate Adsorption Mechanisms at
548 the Ferrihydrite–Water Interface. *Journal of Colloid and Interface Science*, 2001, 241, 317–326.
549 30. Elzinga, E. J. and Sparks, D. L. Phosphate Adsorption onto Hematite: An *in situ* ATR-FTIR Investigation of
550 the Effects of pH and Loading Level on the Mode of Phosphate Surface Complexation. *Journal of Colloid and*
551 *Interface Science*, **2007**, 308, 53–70.
552 31. Zhang, G. Y. and Peak, D. Studies of Cd(II)–Sulfate Interactions at the Goethite-Water Interface by ATR-FTIR
553 Spectroscopy. *Geochimica et Cosmochimica Acta*, **2007**, 71, 2158–2169.
554 32. Davantes, A.; Costa, D.; Lefevre, G., Molybdenum(VI) Adsorption onto Lepidocrocite (gamma-FeOOH): *In*
555 *Situ* Vibrational Spectroscopy and DFT plus U Theoretical Study. *Journal of Physical Chemistry C*, **2016**, 120,
556 11871–11881.
557 33. Yang, Y. L.; Wang, S. R.; Xu, Y. S.; Zheng, B. H.; Liu, J. Y. Molecular-Scale Study of Aspartate Adsorption on
558 Goethite and Competition with Phosphate. *Environmental Science & Technology*, **2016**, 50, 2938–2945.
559 34. Noda, I. Frontiers of Two-Dimensional Correlation Spectroscopy. Part 1. New Concepts and Noteworthy
560 Developments. *Journal of Molecular Structure*, **2014**, 1069, 3–22.
561 35. Noda, I. Frontiers of Two-Dimensional Correlation Spectroscopy. Part 2. Perturbation Methods, Fields of
562 Applications, and Types of Analytical Probes. *Journal of Molecular Structure*, **2014**, 1069, 23–49.
563 36. Yan, W.; Zhang, J.; Jing, C. Adsorption of Enrofloxacin on Montmorillonite: Two-Dimensional Correlation
564 ATR/FTIR Spectroscopy Study. *Journal of Colloid and Interface Science*, **2013**, 390, 196–203.
565 37. Lindegren, M.; Loring, J. S.; Persson, P. Molecular Structures of Citrate and Tricarballylate Adsorbed on alpha-
566 FeOOH Particles in Aqueous Suspensions. *Langmuir*, **2009**, 25, 10639–47.
567 38. Murphy, J. and Riley, J. P. A. Modified Single Solution Method for Determination of Phosphate Uptake by
568 Rye. *Analytica Chimica Acta*, **1962**, 26, 31–36.
569 39. Tiberg, C. and Gustafsson, J. P. Phosphate Effects on Cadmium(II) Sorption to Ferrihydrite. *Journal of Colloid*
570 *and Interface Science*, **2016**, 471, 103–11.
571 40. Gao, Y. and Mucci, A. Acid Base Reactions, Phosphate and Arsenate Complexation, and Their Competitive
572 Adsorption at the Surface of Goethite in 0.7 M NaCl Solution. *Geochimica et Cosmochimica Acta*, **2001**, 65, 2361–
573 2378.

41. Hawke, D.; Carpenter, P. D.; Hunter, K. A. Competitive Adsorption of Phosphate on Goethite in Marine Electrolytes. *Environmental Science & Technology*, **1989**, 23, 187–191.
42. Eggleston, C. M.; Hug, S.; Stumm, W.; Sulzberger, B.; Afonso, M. D. S. Surface Complexation of Sulfate by Hematite Surfaces: FTIR and STM Observations. *Geochimica et Cosmochimica Acta*, **1998**, 62, 585–593.
43. Hug, S. J. *In situ* Fourier Transform Infrared Measurements of Sulfate Adsorption on Hematite in Aqueous Solutions. *Journal of Colloid and Interface Science*, **1997**, 188, 415–422.
44. Collins, C. R.; Ragnarsdottir, K. V.; Sherman, D. M. Effect of Inorganic and Organic Ligands on the Mechanism of Cadmium Sorption to Goethite. *Geochimica et Cosmochimica Acta*, **1999**, 63, 2989–3002.
45. Johnston, C. P. and Chrysochoou, M. Investigation of Chromate Coordination on Ferrihydrite by in situ ATR-FTIR Spectroscopy and Theoretical Frequency Calculations. *Environmental science & technology*, **2012**, 46, 5851–5858.
46. Tejedor-tejedor, M. I. and Anderson, M. A. Protonation of Phosphate on the Surface of Goethite as Studied by CIR-FTIR and Electrophoretic Mobility. *Langmuir*, **1990**, 6, 602–611.
47. Persson, P.; Nilsson, N.; Sjöberg, S. Structure and Bonding of Orthophosphate Ions at the Iron Oxide–Aqueous Interface. *Journal of Colloid and Interface Science*, **1996,** 177, 263–275.
48. Farley, K. J.; Dzombak, D. A.; Morel, F. M. A. Surface Precipitation Model for the Sorption of Cations on Metal Oxides. *Journal of Colloid and Interface Science*, **1985**, 106, 226–242.
49. Swedlund, P. J.; Webster, J. G.; Miskelly, G. M. Goethite Adsorption of Cu(II), Pb(II), Cd(II), and Zn(II) in the Presence of Sulfate: Properties of the Ternary Complex. *Geochimica et Cosmochimica Acta*, **2009**, 73, 1548–1562.
50. Wang, K. and Xing, B. Mutual effects of Cadmium and Phosphate on Their Adsorption and Desorption by Goethite. *Environmental Pollution*, **2004**, 127, 13–20.
51. Hoins, U.; Charlet, L.; Sticher, H. Ligand Effect on the Adsorption of Heavy Metals: The Sulfate-Cadmium-Goethite Case. *Water, Air, & Soil Pollution*, **1993**, 68, 241–255.
52. Wijnja, H. and Schulthess, C. P. Vibrational Spectroscopy Study of Selenate and Sulfate Adsorption Mechanisms on Fe and Al (hydr)oxide Surfaces. *Journal of Colloid and Interface Science*, **2000**, 229, 286–297.
53. Lefevre, G. and Fédoroff, M. Sorption of Sulfate Ions onto Hematite Studied by Attenuated Total Reflection-Infrared Spectroscopy: Kinetics and Competition with Other Ions. *Physics and Chemistry of the Earth, Parts A/B/C*, **2006**, 31, 499–504.
54. Paul, K. W.; Borda, M. J.; Kubicki, J. D.; Sparks, D. L. Effect of Dehydration on Sulfate Coordination and Speciation at the Fe–(hydr)oxide–Water Interface: A Molecular Orbital/Density Functional Theory and Fourier Transform Infrared Spectroscopic Investigation. *Langmuir*, **2005**, 21, 11071–11078.
55. Zhu, M.; Northrup, P.; Shi, C.; Billinge, S. J.; Sparks, D. L.; Waychunas, G. A. Structure of Sulfate Adsorption Complexes on Ferrihydrite. *Environmental Science & Technology Letters*, **2013**, 1, 97–101.
56. Gu, C.; Wang, Z.; Kubicki, J. D.; Wang, X.; Zhu, M. X-ray Absorption Spectroscopic Quantification and Speciation Modeling of Sulfate Adsorption on Ferrihydrite Surfaces. *Environmental Science & Technology*, **2016**, 50, 8067–8076.
57. Hinkle, M. A.; Wang, Z.; Giammar, D. E.; Catalano, J. G. Interaction of Fe(II) with Phosphate and Sulfate on Iron Oxide Surfaces. *Geochimica et Cosmochimica Acta*, **2015**, 158, 130–146.
58. Singh, A.; Catalano, J. G.; Ulrich, K. U.; Giammar, D. E. Molecular-Scale Structure of Uranium (VI) Immobilized with Goethite and Phosphate. *Environmental Science & Technology*, **2012**, 46, 6594–6603.

617 Table 1. Summary of the sulfate IR bands in the ATR-IR experiments.

System	Species	v_3 bands position (cm^{-1})		
S-pH 7	OS	1100		
	C_{2v}	1155	1140	1048
S-pH 5	OS	1100		
	C_{2v}	1150	1130	1047
S+Cd-pH 9	OS	1105		
	C2v	1155	1130	1050
	C3v	1130	1075	(1030)
S+Cd-pH 7	OS	1105		
	C_{2v}	1155	1130	1060
	C_{3v}	1130	1085	(1030)
S+Cd-pH 5	OS	1105		
	C_{2v}	1160	1130	1060
	C_{3v}	1130	1085	(1020)

618 OS represents the outer-sphere complexes; C_{2v} and C_{3v} denote the complexes with symmetry of C_{2v} and C_{3v},
619 respectively.

620

621 Table 2. Summary of the phosphate IR bands in the ATR-IR experiments.

System	Species	ν_3 bands position (cm^{-1})		
P-pH 9	C_{2v}	1075	1025	950
P-pH 7	C_{2v}	1075	1035	945
	C_{3v}	1100	970	
P-pH 5	C_{2v}	1075	1025	945
	C_{2v}	1105	1050	995
P+Cd-pH 9	C_{2v}	1118	1070	975
	C_{2v}	1090	1033	936
P+Cd-pH 7	C_{2v}	1125	1000	945
	C_{2v}	1075	1025	975
	C_{3v}	1075	1010	
P+Cd-pH 5	C_{2v}	1128	1062	995
	C_{2v}	1080	1045	935
	C_{3v}	1100	970	

622

623

Table 3. The offset values of pH_{50} (the difference of pH values at which 50% of the Cd(II) was adsorbed in the absence and presence of ligands) in pH adsorption edges in the co-adsorption studies of Cd(II) and ligands (sulfate or phosphate).

Offset of pH_{50}	**C_{Cd} (mM)**	**C_S (mM)**	**I (mM)**	**D_{Fh} (g/L)**	**D_{Gt} (g/L)**	**Q_{Cd} (μmol/g)**	**Reference**
0.6	0.07	10	100		1.4	25	49
0.5	0.07	2	100		1.4	25	49
0.8	0.03	2	10		12.5	1.2	51
0.4	0.01	10	100	1		5	20
0.4	0.1	10	100	1		50	20
1	0.2	0.5	1	2.5		40	this study
1.4	0.2	1	1	2.5		40	this study
2	0.2	2	1	2.5		40	this study
Offset of pH_{50}	**C_{Cd} (mM)**	**C_P (mM)**	**I (mM)**	**D_{Fh} (g/L)**	**D_{Gt} (g/L)**	**Q_{Cd} (μmol/g)**	**Reference**
1.2	0.03	0.6	10	0.3		50	39
2	0.01	1	10		10	0.5	50
1	0.2	0.5	1	2.5		40	this study
1.3	0.2	1	1	2.5		40	this study
2	0.2	2	1	2.5		40	this study

D_{Fh} and D_{Gt} represent the dosages of Fh and goethite, respectively; C_{cd}, C_P, and C_S denote the concentrations of Cd(II), phosphate and sulfate, respectively; I represents the ionic strength; Q_{Cd} (the adsorbed amount of Cd(II)) was estimated from data in the given reference.

Figure 1. Adsorption isotherms (A) of Cd(II) in the absence or presence of sulfate (S) or phosphate (P) (Numbers in the legend denote that the initial concentrations of S or P were of 0.5, 1, or 2 mM; the concentrations of Cd(II) were of 0.2−2 mM in the adsorption isotherms and 0.2 mM in the pH adsorption edges); the percentages of desorbed Cd(II), S, and P by equilibrating with 0.3 M NaCl (B). (No phosphate was desorbed in the desorption experiment)

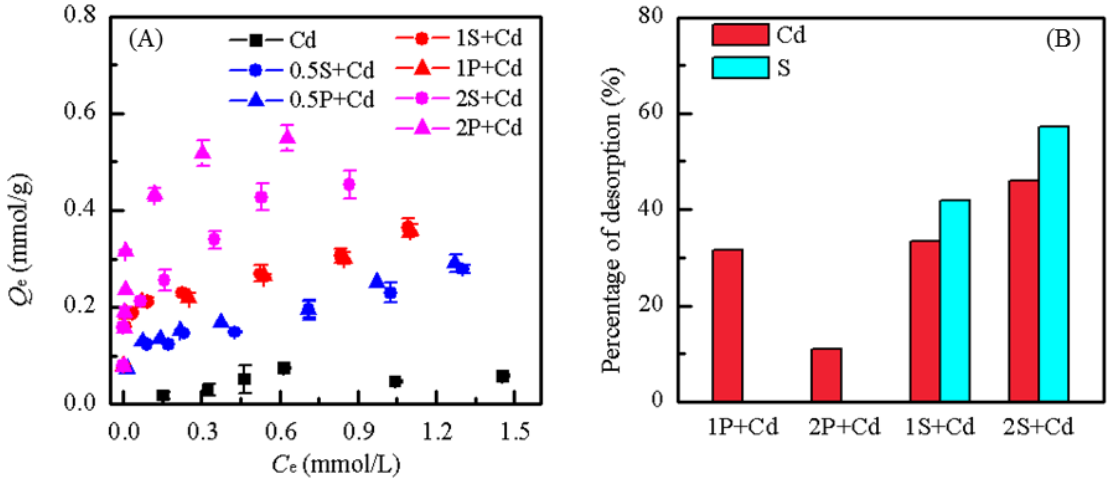

Figure 2. The adsorption of Cd(II) at varied pH in the absence or presence of S or P (A); the Cd(II) speciation in the presence of 1 or 2 mM S (B) or P (C) (denoted as “Cd+1S or P” or “Cd+2S or P” system) calculated using visual MINTEQ (the concentrations of Cd(II) and oxyanions were set the same as those in the pH adsorption edges).

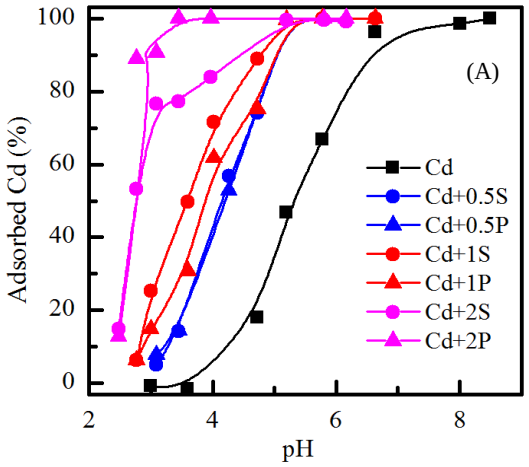

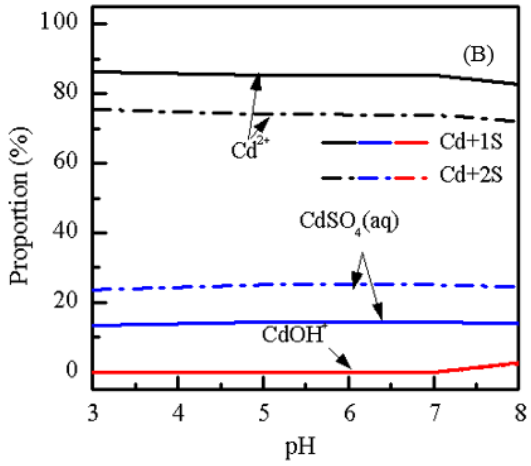

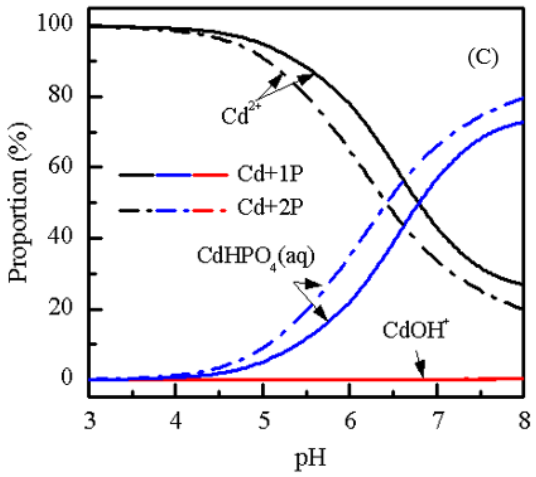

Figure 3. Infrared spectra of sulfate at the water-Fh interface at pH 5–9 in S systems (A) and S+Cd systems (C); synchronous (red images) and asynchronous (colored images) contour plots obtained from the 2D-COS analysis of the infrared spectra of sulfate adsorbed on Fh at pH 9, pH 7 and pH 5 in S systems (B) and S+Cd systems (D). (In the colored images: from green to red, the values of z are positive, while from green to blue, the values are negative). Since the adsorbed amount of sulfate at pH 9 was too small to obtain a series of spectra as a function of time, the 2D contour plots of the S-pH 9 system could not be obtained.

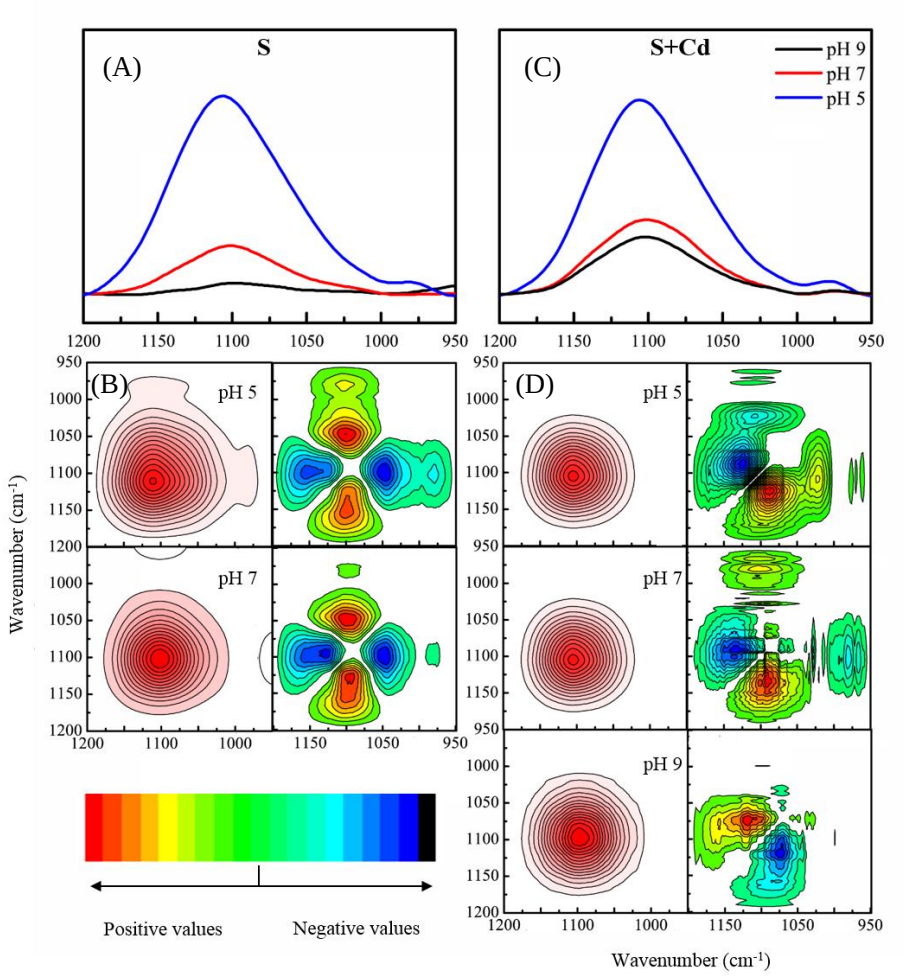

Figure 4. Proposed configurations of the sulfate–Cd complexes (A and B). Cd surface complexes are in octahedral coordination with O ligands according to previous studies.[44]

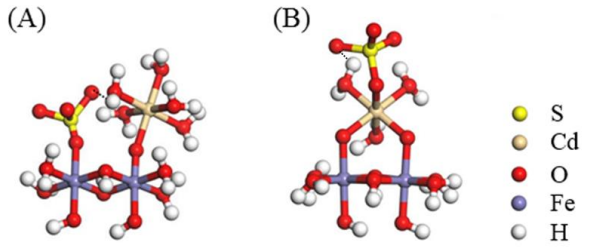

Figure 5. Infrared spectra of phosphate at the water-Fh interface at pH 5−9 in P systems (A) and P+Cd systems (C); synchronous and asynchronous contour plots obtained from the 2D-COS analysis of the infrared spectra of phosphate adsorbed on Fh at pH 9, pH 7, and pH 5 in P systems (B) and P+Cd systems (D).

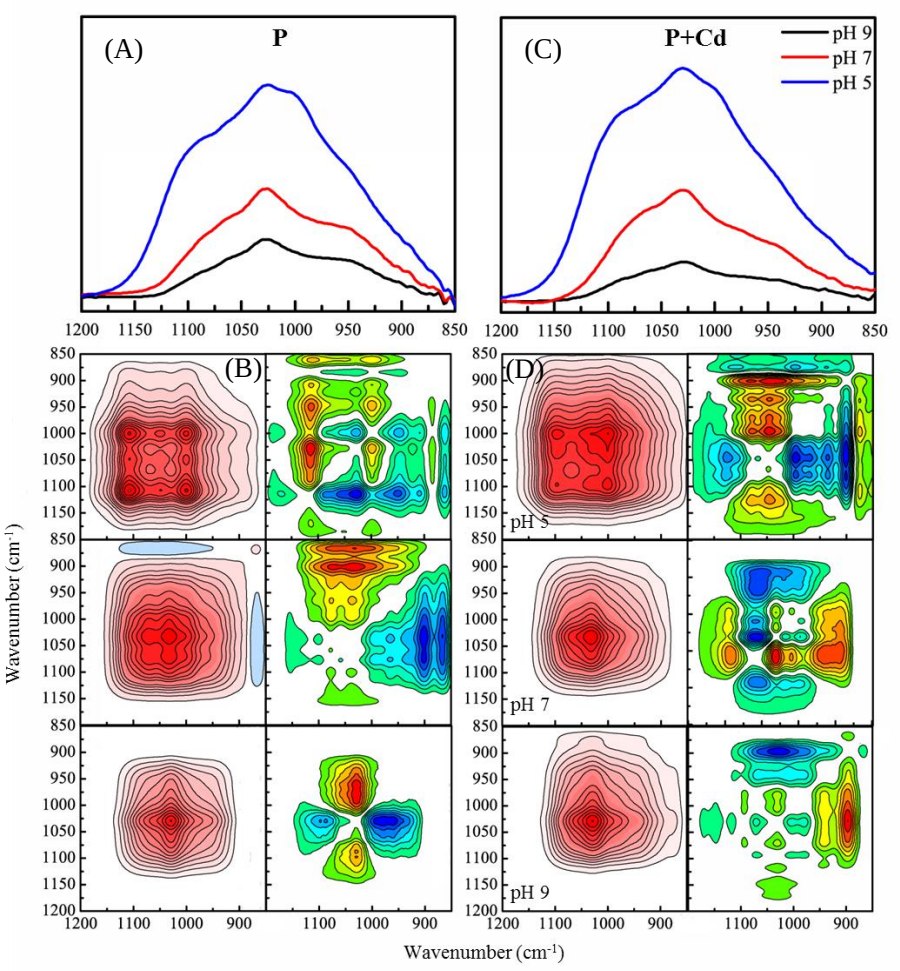

Figure 6. Proposed configurations of the phosphate–Cd (A and B) complexes in the co-adsorption systems.